Cumhuriyet Sci. J., 45(3) (2024) 510-518
DOI: https://doi.org/10.17776/csj.1234262

Cumhuriyet Science Journal

| csj.cumhuriyet.edu.tr | Founded: 2002 ISSN: 2587-2680 e-ISSN: 2587-246X Publisher: Sivas Cumhuriyet University

Engineering Zinc Ion Hybrid Supercapacitor Performance of Graphitic Carbon Nitride Embedded Iron Oxide (Hematite)

Sevda Yetiman[1,a], Fatma Kılıç Dokan[2,b,*], Dilek Aker[1,3,c], Ahmet Turan Ozdemir [4,d], Mustafa Serdar Onses [1,5,e], Erkan Yılmaz [1,6,f], Ertugrul Sahmetlioglu[1,7,g]

[1] ERNAM-Erciyes University Nanotechnology Application and Research Center, Kayseri, 38039, Türkiye
[2] Department of Chemistry and Chemical Processing Technologies, Mustafa Çıkrıkcıoglu Vocational School, Kayseri University, Kayseri, Türkiye
[3] Department of Nuclear Technology and Radiation Safety, School of Health Services, Uskudar University, İstanbul, Türkiye
[4] Department of Electrical and Electronics Engineering, Erciyes University, 38039, Kayseri, Türkiye
[5] Department of Materials Science and Engineering, Faculty of Engineering, Erciyes University, 38039, Kayseri, Türkiye
[6] Technology Research & Application Center (TAUM), Erciyes University, Kayseri, 38039, Türkiye
[7] Department of Basic Sciences of Engineering, Kayseri University, 38039, Kayseri,Türkiye
**Corresponding author*

Research Article

History
Received: 02/12/2022
Accepted: 20/08/2024

ABSTRACT

Zinc-ion hybrid supercapacitors (ZHSC) gain high traction due to the prosperous unification of batteries and supercapacitors. Especially with graphene discovery nano carbonaceous materials have been the most investigated types in energy storage (ES) utilization including ZHSC. Among carbonaceous materials, graphitic carbon nitride (g-C_3N_4) possessing polymeric layers, quasi graphene arouses extreme interest due to its low-impact structure with economical yet chemical and mechanical stability inflicted by high nitrogen contents. Herein, we aim to examine the g-C_3N_4 doping effect on the electrochemical performance of hematite (α-Fe_2O_3) for ZHSC application. The assembled ZHSC device managed to reach the potential window of 2.0 volts with an efficient specific capacitance (Sc) of 280 F g^{-1} at a current density of 1 A g^{-1}. Moreover, the highest energy and power densities were 38.8 Wh kg^{-1} and 20 kW kg^{-1} respectively. With this remarkable efficiency, the α-Fe_2O_3/g-C_3N_4 composite material can be considered a promising cathode material for ZHSC.

Keywords: Graphitic carbon nitride, Iron (III) oxide, Zinc-ion hybrid supercapacitor.

[a] *ytmnsevda@gmail.com* *https://orcid.org/0000-0002-8558-8688*
[c] *dilek.aker@uskudar.edu.tr* *https://orcid.org/0000-0003-3407-2750*
[e] *onses@erciyes.edu.tr* *https://orcid.org/0000-0001-6898-7700*
[g] *sahmetlioglu@kayseri.edu.tr* *https://orcid.org/0000-0002-7324-0385*
[b] *fatmakilic@kayseri.edu.tr* *https://orcid.org/0000-0002-5355-2904*
[d] *aturan@erciyes.edu.tr* *https://orcid.org/0000-0002-2796-1384*
[f] *erkanyilmaz@erciyes.edu.tr* *https://orcid.org/0000-0001-8962-3199*

Introduction

Regarding the ongoing increase in energy consumption, it is crucial to diversify energy resources that are susceptible to depletion and to create efficient ES systems for future utilization. Supercapacitors (SCs) are among the most imminent electrochemical ES devices for future energy systems due to their almost unlimited lifespan,charge-discharge capability, and excellent power density. However, the low energy density (ED) of SCs is the main disadvantage limiting their utilization [1-14]. The specific capacity can be boosted by battery-like redox reactions, although, the aqueous electrolyte's voltage window is restricted by water decomposition. Therefore, improving the voltage window of aqueous SCs is crucial to obtaining high-performance SCs.

Recently, there has been a growing interest in metal ion hybrid devices, such as those containing lithium (Li), aluminium (Al), potassium (K), magnesium (Mg), and zinc (Zn) metals [3, 15, 16]. These devices combine a battery-like anode with a cathode that exhibits pseudocapacitive properties, such as metal oxides, sulfides, or conductive polymers. Zinc-ion hybrid batteries (ZIHB) and zinc-ion hybrid supercapacitors (ZHSC) are prominent ion hybrid systems that excel in terms of their high capacity (819 mAh g^{-1}) and low redox potential (Zn/Zn^{2+}) (0.78 V against Standard Hydrogen Electrode, SHE). These characteristics are crucial for improving the ED of ES devices. In addition, Zn is a more affordable and abundant metal (about 300 times greater than Li) that is also more reliable for usage in aqueous-based electrochemical systems compared to Li, Na, and K[11, 17].

Up to date, various materials have been utilized as cathode material for SCs and ZHSCs applications including especially carbon-based materials. Among carbonaceous materials, graphitic carbon nitride (g-C_3N_4) with polymeric layers, also known as quasi graphene, has piqued the interest of researchers due to its low-impact structure with no cost effect, as well as the chemical and mechanical durability conferred by high nitrogen content [18, 19].

For instance, Zhou et al. formed flower-shaped PANI/g-C_3N_4 hybrid material given the maximal Sc of 584.3 F g^{-1}, and the Sc degradation was just ~ 8 % after 1000 cycles [20]. Ragupathi et al. analyzed MnS electrochemical features with the g-C_3N_4 effect and reported the highest

Sc of 463.32 F g^{-1} at the scan rate of 10 mV s^{-1} with 98.6 % retention after 2000 cycles [21] .

Herein, we aim to utilize the synergic effect of α-Fe_2O_3 and g-C_3N_4 for high-performance ZHSC. In the first step, the electrochemical features of α-Fe_2O_3 and g-C_3N_4 were scrutinized in three electrode system. When the Sc of pure α-Fe_2O_3 at a current density of 1 A g^{-1} was 184 F g^{-1}, hybrid material achieved 438 F g^{-1} capable of operating at high rates even at 20 A g^{-1}. Moreover, the hybrid material's cyclic stability was also better than pristine α-Fe_2O_3, the degradation was 25 % while the degradation of the Sc of α-Fe_2O_3/g-C_3N_4 was 15 % after 5000 continuous cycles. Afterward, the best-yielded composite electrode was formed as the cathode electrode for ZHSC. The maximal Sc was 280 F g^{-1} at the current density of 2.5 A g^{-1} when the highest ED and PD were 38.8 Wh kg^{-1}, and 20 kW kg^{-1}, respectively. Considering these excellent findings, the resulting hybrid material is a viable cathode material for aqueous ZHSCs.

Materials and Methods

Materials

Iron (III) chloride ($FeCl_3$, 99.0 %), sodium sulfate (Na_2SO_4, ≥ 99.0 %), urea ($CO[NH_2]_2$, 98.0 %),potassium hydroxide (KOH, ≥ 85.0 %) nitric acid (HNO_3, 65.0%) were purchased from Merck (GERMANY). Sigma-Aldrich (USA) was the supplier company for polyvinylidene fluoride (PVDF, 99.9 %) and n-methyl-2-pyrrolidone (NMP, 99.0 %). All chemical reagents and solvents for synthesis and analysis were utilized without further purification and the used deionized water (DI) was 18.2 MΩ cm resistivity.

Synthesis of α-Fe_2O_3

In particular, 3 mmol $FeCl_3$ was dissolved DI. After adding 1.6 mmol of Na_2SO, this mixture was ultrasonically sonicated for 1.5 hours. The resulting dark brown solution underwent a six-hour hydrothermal treatment at 120 °C. To get pure α-Fe_2O_3, the particles were centrifuged, washed with DI and ethanol, vacuum dried at 90°C for 15 hours, then calcined at 450°C for 2.5 hours at a rate of 1°C min^{-1} in flowing air[22].

Synthesis of g-C_3N_4

In a typical method, bulk g-C_3N_4 powders were obtained after calcining 10 g urea for 4 h at 550°C at 30°C min^{-1} heating rate in air in an enclosed muffle furnace. The obtained bulk g-C_3N_4 particles were then mixed magnetically in 50 mL of HNO_3 (pH-1) aqueous solution and heated to 90 °C for 8 hours. The sample was cleaned with DI and ethanol to eliminate contaminants and bring the pH level to 7, then vacuum dried for 15 hours at 85°C. The acquired yellowish product was stored in a desiccator pending use[23] .

Structural Characterization

The crystallographic conformation of the materials was investigated using a Bruker AXS D8 X-ray powder diffractometer with a simple cubic lattice and CU K radiation (λ = 0.15 nm), with the scan range (2θ) varying from 5° to 90°. Fourier Transform Infrared Spectroscopy (FTIR, Spectrum Two, Perkin-Elmer, USA) was applied to screen the chemical bonds of the molecules. The materials' morphology was examined using a Field Emission Scanning Electron Microscope (FE-SEM, Gemini 550) and a Scanning Transmission Electron Microscope (STEM, Gemini 550). Brunauer-Emmett-Teller (BET), and (Barrett-Joyner-Halenda) BJH methods (Micromeritics, Gemini Vii) were performed to obtain the pore size distribution, total pore volume (TPV), and the specific surface area (SSA) of the materials.

Electrochemical Characterization

Electrode fabrication and Tests

The electroactive materials (α-Fe_2O_3, α-Fe_2O_3/g-C_3N_4: 85 wt %, acetylene black: 10 wt %, and PDVF:5 wt % were ultrasonicated in few drops of NMP solvent. Nickel foam (NF) (1cm × 1cm) was chosen as the current collector. The electroactive materials' slurry was dropped onto the NF and vacuum dried at 95 °C for 12 h.When the active components were obtained, they weighed around 1.5 mg.

Gamry Referance, 3000 Electrochemical Workstation was utilized to check the cyclic voltammetry (CV), galvanostatic charge-discharge (GCD), and electrochemical impedance spectroscopy (EIS) measurements. All three electrode analyses were managed in 2M KOH aqueous electrolytes by using the obtained materials as working electrodes, when silver /silver chloride (Ag/AgCl), and platinum (Pt) foil (1x1cm) were the reference, counter electrodes, respectively.

The following equations were used to measure the Sc values of the electrodes at different scan rates, and current densities

$$Sc = \frac{\int \mathrm{I(V)\,dV}}{\mathrm{v\ x\ m\ x\ \Delta V}} \tag{1}$$

$$Sc = \frac{\mathrm{I\ x\ \Delta t}}{\mathrm{m\ x\ \Delta V}} \tag{2}$$

Where Sc (F g^{-1}), $\int$ I(V) dV,v(mV s^{-1}), m(g), ΔV (V), I (A), Δt (s) indicate the specific capacitance, the area under the CV curve, scan rate, mass of the active material, potential window, discharge current and, the average discharge time, respectively.

The energy density (E,Wh kg^{-1}), and the power density (P, W kg^{-1}) were measured according to the following formulas:

$$E = \frac{\mathrm{Ccell\ x\ \Delta V}^{2}}{\mathrm{2\ x\ 3.6}} \tag{3}$$

$$P = \frac{\mathrm{3600\ x\ E}}{\mathrm{\Delta t}} \tag{4}$$

Fabrication of ZHSC device

ZHSC was formed by using α-Fe_2O_3@g-C_3N_4 as cathode, Zn foil as both the anode and current collector in 2M KOH + 0.05 M $ZnSO_4$ electrolyte at a potential range of 1.0-2.0 V. Equations (2), (3), and (4) were used to measure the Sc (F g^{-1}), the Ed (E, Wh kg^{-1}), and the Pd (P, W kg^{-1}) of the ZHSC device.

Results and Discussion

Structural and Morphological Studies

X-ray diffraction (XRD) analysis was performed to check the formation and phase character of the patterns. In Figure 2a the peaks detected at 25.50° (012),34.56°(104), 37.04°(110),41.61°(113), 49.91°(024), 55.24°(116),58.14°(018), 65.2°(214) and, 68.4°(300) are the characteristic peaks of α-Fe_2O_3 (JPCDS card no. 33-0664) [11, 15, 24]. In Figure 1a the peaks at 2Ɵ values of 13.24° and 27.71° are diacritical peaks of the (100) and (002) planes of g-C_3N_4 and observed all idiosyncratic peaks of α-Fe_2O_3 indicate α-Fe_2O_3/g-C_3N_4 composite was formed successfully [20, 21].

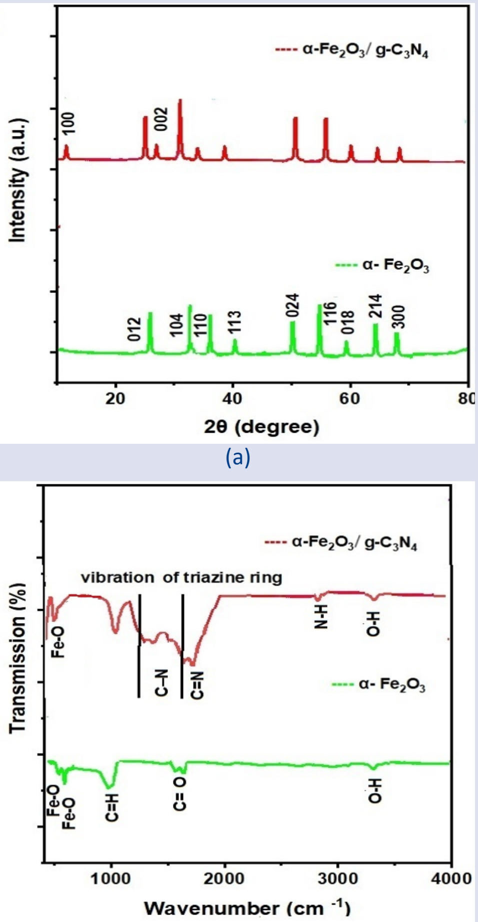

(a)

(b)

Figure 1. Structural characterization. (a) XRD patterns, and (b) FTIR spectra of α-Fe_2O_3, α-Fe_2O_3/g-C_3N_4.

FTIR screening was carried out to investigate the chemical production and chemical bonding of the components. In Figure 1b (green line). the broad band at 3450 cm^{-1} is considered to be the O-H stretching vibration. The peaks depicted at 1640 cm^{-1} and 1520 cm^{-1} own symmetric and asymmetric bending vibration of C=O. The peak at 895 cm $^{-1}$ belongs to C-H stretching vibration, and Fe-O stretching peaks were monitored at 480 and 562 cm^{-1} [25]. The presence of carbon peaks observed in the FTIR analysis, despite the absence of carbon-containing compounds in the structure, can be attributed to impurities introduced during the measurement or the carbon content present in the environment during the calcining process. In Figure 1b (red line) vibrational peaks of s-triazine units were observed at 821 cm^{-1}. The large peaks in the area of 1250-1620 cm^{-1} belong to C-N stretching vibration of the heterocyclic ring. The peak at 1648 cm^{-1} is associated with the C=N stretching vibration mode, whereas the wide peaks oriented at 2980 cm^{-1} and 3467 cm^{-1} might be related to the N-H and O-H vibrations [23, 26-28]. The screened distinct peaks of α-Fe_2O_3 demonstrate that the α-Fe_2O_3/g-C_3N_4 combination prosperously formed.

The pore chemistry of the patterns was determined by N_2 adsorption-desorption isotherms (Figure 2). The specific surface areas (SSA) and total pore volume (TPV) of α-Fe_2O_3, α-Fe_2O_3/g-C_3N_4, are 5.66m^2 g^{-1} ; 0.031 cm^3 g^{-1}, 11.92 m^2 g^{-1}; 0.076 cm^3/g respectively. The SSA of α-Fe_2O_3 was enhanced and nearly doubled, thanks to the high porosity structure of g-C_3N_4, α-Fe_2O_3/g-C_3N_4 composite has the highest pore volume (2~ wider than pristine α-Fe_2O_3).

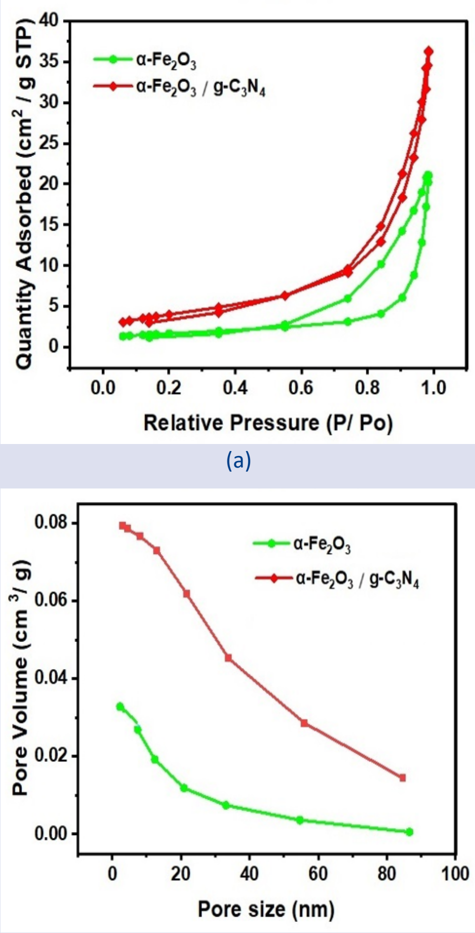

(a)

(b)

Figure 2. (a) Nitrogen adsorption-desorption isotherms of α-Fe_2O_3, α-Fe_2O_3/g-C_3N_4, and (b) BJH size distribution plots of the patterns.

In Figure 3 the surface morphology of the samples examined by FESEM and STEM are presented. In Figure 3 [20] FESEM and STEM images of nanowire α-Fe_2O_3 are shown which are dismantled with the addition of g-C_3N_4 as seen in Figure 4 (c- d). Agglomerated and interwoven particles also confirm the successful combination of the materials.

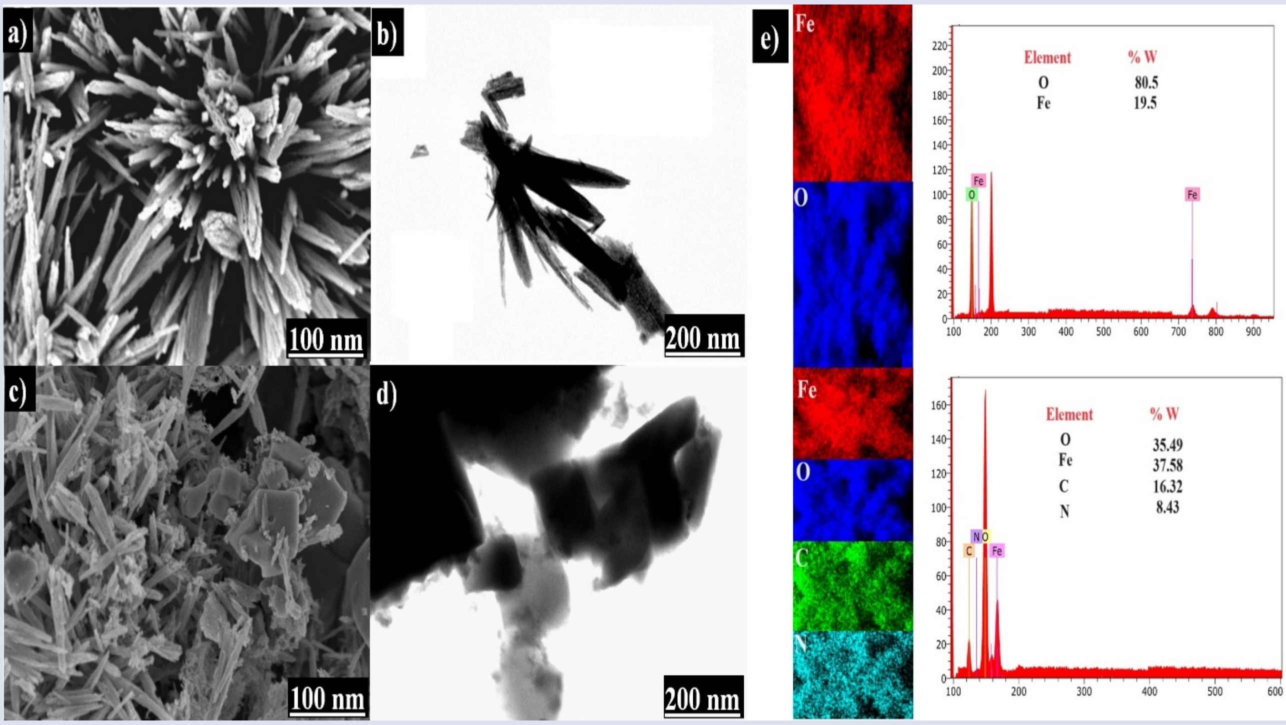

Figure 3. FESEM and STEM images of the samples. [20] α-Fe_2O_3 and, (c-d) α-Fe_2O_3/g-C_3N_4. (e) Individual elemental mapping images of Fe, O, C, N,and spectra of EDX, respectively.

Electrochemical Studies

Cyclic voltammetry studies

The electrochemical characterization findings are displayed in Figure 4. Figure4 (a-b) displays the individual CV curves for each material at various scan rates (20-50-100 mV s^{-1}).

The area under the CV curves expands with the increase in scan rates yet all samples still exhibit obvious redox peaks. The Sc of the electrodes with discrete scan rates was reckoned according to the equation (1). It can be syllogized that the oxidation and reduction peaks of α-Fe_2O_3/g-C_3N_4 are more distinct and the area under the CV curve is wider (Figure 4a) [29-31]. The obtained highest Sc of α-Fe_2O_3 and α-Fe_2O_3/g-C_3N_4 are 177 g^{-1}and 326 F g^{-1} in 2 M KOH at a scan rate of 5 mV s^{-1}. The other Sc variations with different scan rates are exhibited in Figure 5a.

Chronopotentiometry

Charge-discharge performance and stability after long cycles of the electrodes after extended cycles at various current densities at different current densities (1 Ag^{-1}-20 Ag^{-1}) were checked by implementing GCD measurements.

The proper potential window for the electrodes was -0.1 to 0.40 V (vs. Ag/AgCl) in 2M KOH aqueous electrolyte. On one hand, at low current densities more electroactive interference between the electrode surface and OH^{-1} ions causes an increment on specific capacitance. On the other hand, at high current density low interaction causes a decrease on the specific capacitances.

Individual GCD curves and Sc variation with different current densities are shown in Figure 4(c-d), and Figure 5(b). The highest Sc, calculated via equation (2), for all electrodes are obtained at a current density of 1 A g^{-1}. We can declare that with the addition of g-C_3N_4 charge-discharge time of α-Fe_2O_3 increased significantly. Therefore, the composite α-Fe_2O_3/g-C_3N_4 has higher Sc at the same current densities as shown in Figure (5b).

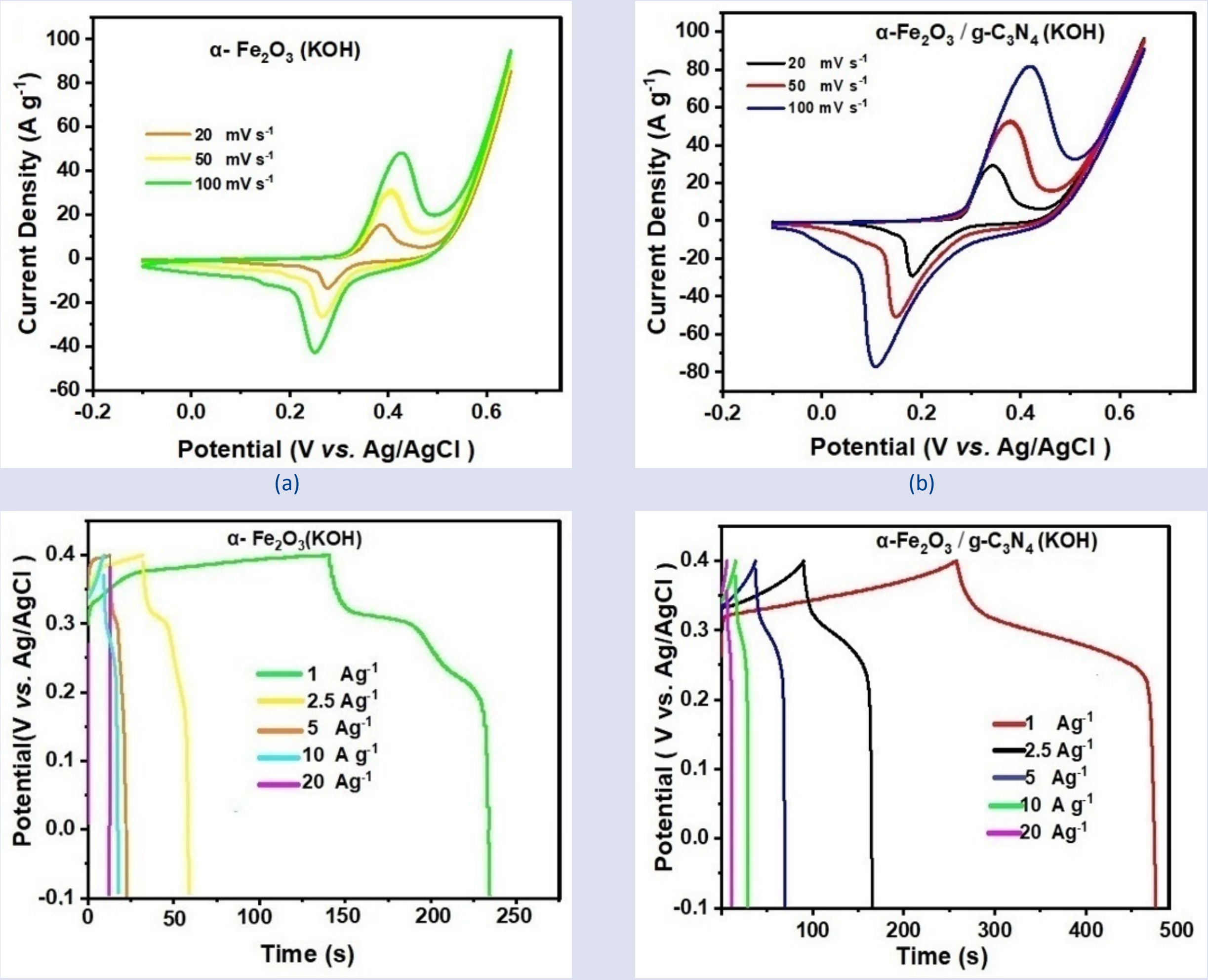

(a) (b)

(c) (d)

Figure 4. Electrochemical measurement results of the α-Fe_2O_3, and α-Fe_2O_3/g-C_3N_4. [20] CV curves, (c-d) GCD curves.

As shown in Figure 5(c) a long-term chronopotentiometry experiment at a current density of 20 Ag^{-1} for up to 5000 cycles was undertaken to further investigate the electrodes' long-term cyclic stability. When the retention of α-Fe_2O_3 were 75 % ,the retention of α-Fe_2O_3/g-C_3N_4 were 85% in 2M KOH electrolyte indicating g-C_3N_4 addition improve the cyclic stability of α-Fe_2O_3.

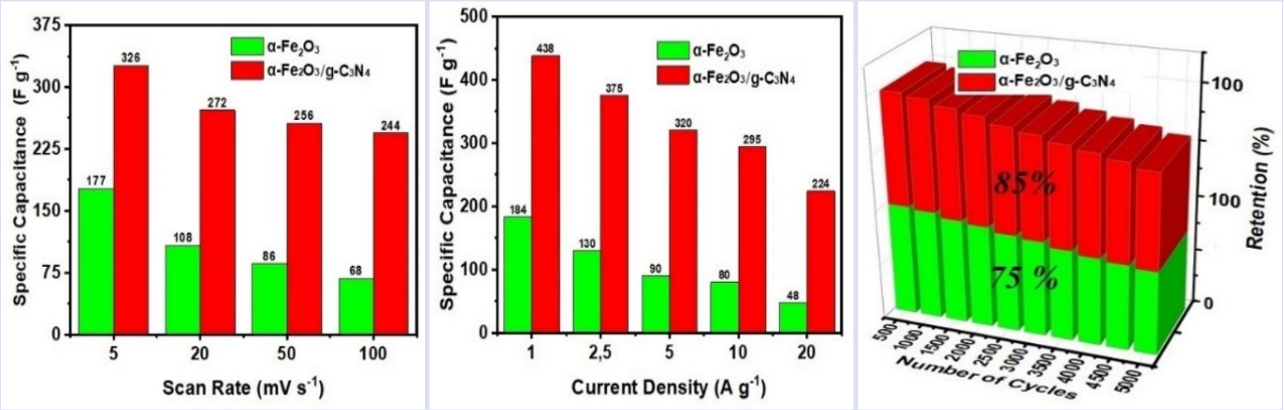

(a) (b) (c)

Figure 5. (a) Sc variation with different scan rates, (b) GCD curves, (c) Long term cyclic stabilities after 5000 cycles.

Electrochemical impedance spectroscopy (EIS)

The electrochemical impedance spectroscopy (EIS) was used to examine the kinetics of ion and charge transmission behavior of the electrodes at high and low frequencies ranging from 0.01 to 100 kHz. The low-frequency area controls the barrier to ion diffusion while the high-frequency region specifies the charge transmission [32, 33].

Ion diffusion between the electro-active area of the electrode and electrolyte intersection generates an extra line entitled the Warburg line. In Figure 6 the Nyquist plots of α-Fe_2O_3 and, α-Fe_2O_3/g-C_3N_4 are illustrated. It is possible to deduce that α-Fe_2O_3 has the lowest charge transport resistance (Rct) and equivalent series resistance (Rs), which rose with the addition of g-C_3N_4, showing that N-inclusive functional groups aroused extra resists.

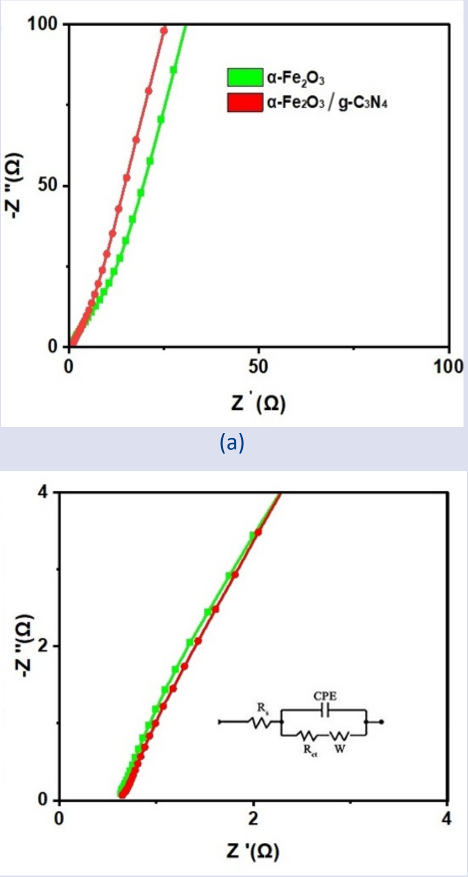

(a)

(b)

Figure 6. Nyquist plots at low (a) and high (b) frequency (The inset shows the zoom-in of Nyquist plots and, equivalent circuit model).

Electrochemical performances of the Zinc-ion hybrid supercapacitor

The formation of a highly efficient ZHSC device was achieved through the consolidation of a battery-type zinc anode and an α-Fe_2O_3/g-C_3N_4 cathode in a 2M KOH + 0.05 M $ZnSO_4$ electrolyte within the potential range of 1.0-2.0V. Figure 7 (a) shows the symbolic representation of the ZHSC device. Figure 7 (b) displays the CV curves of the device at various scan rates. The obvious redox peaks confirm the device has a high pseudocapacitive nature. The Scs of the device were measured by Equation (2). When the recorded highest Sc was 280 F g^{-1} at the current density of 2.5 A g^{-1}, the minimum Sc was 80 F g^{-1} at the current density of 40 A g^{-1}. In Figure 7 (c) GCD curves with various current densities are shown. After 10000 continuous cycles, the retention was 74%.

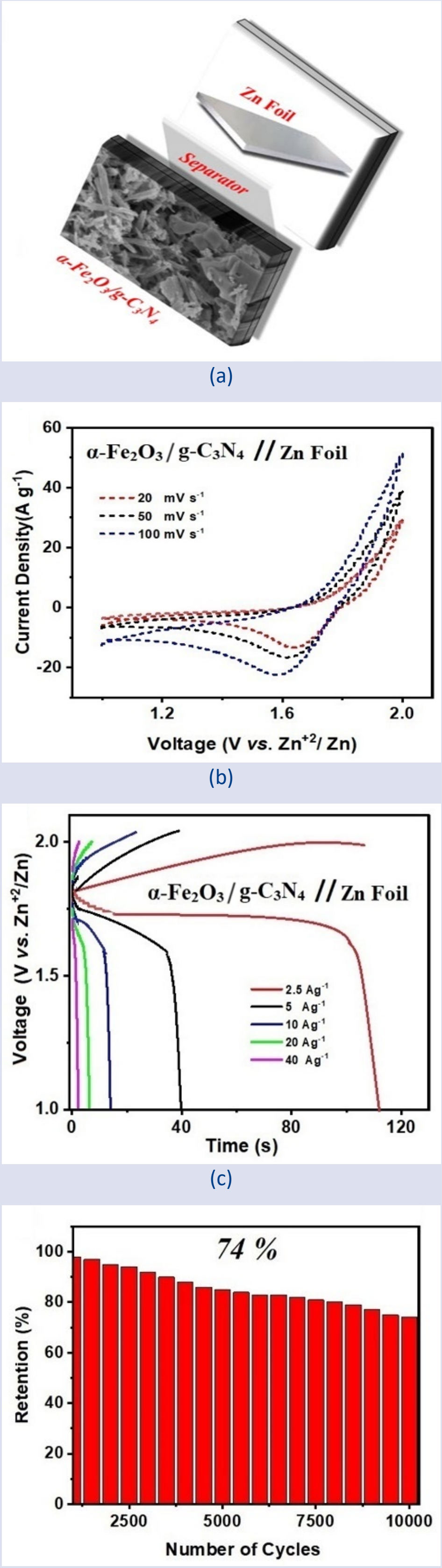

(a)

(b)

(c)

(d)

Figure 7. Electrochemical performance of the ZHSC device. (a) schematic representation of the ZHSC device, (b) CV curves at various scan rates of the ZHSC device, (c) GCD curves at various current densities of the ZHSC, (d) Long term cyclic stability after 10000 cycles.

The Nyquist plot in Figure 8 (a) notes that the device owns a low Rs of 3.2 Ω, and Rct of 3.8 Ω. The Ragon plot indicates the ED and PD of the ZHSC are in the region of the ionic supercapacitor, as seen in Figure 9 (b). In Table 1 the ED (E, Wh kg^{-1}), and the PD (P, W kg^{-1}) of the ZHSC device is recorded. The obtained results are comparable or better than the previously documented outcomes for α-Fe_2O_3 symmetric and asymmetric supercapacitor (SSC , ASC) devices. These results are summarized in Table 2, which includes information on the SC (device), electrolyte, potential range (V), ED (Wh kg^{-1}), PD (W kg^{-1}), and cyclic stability.

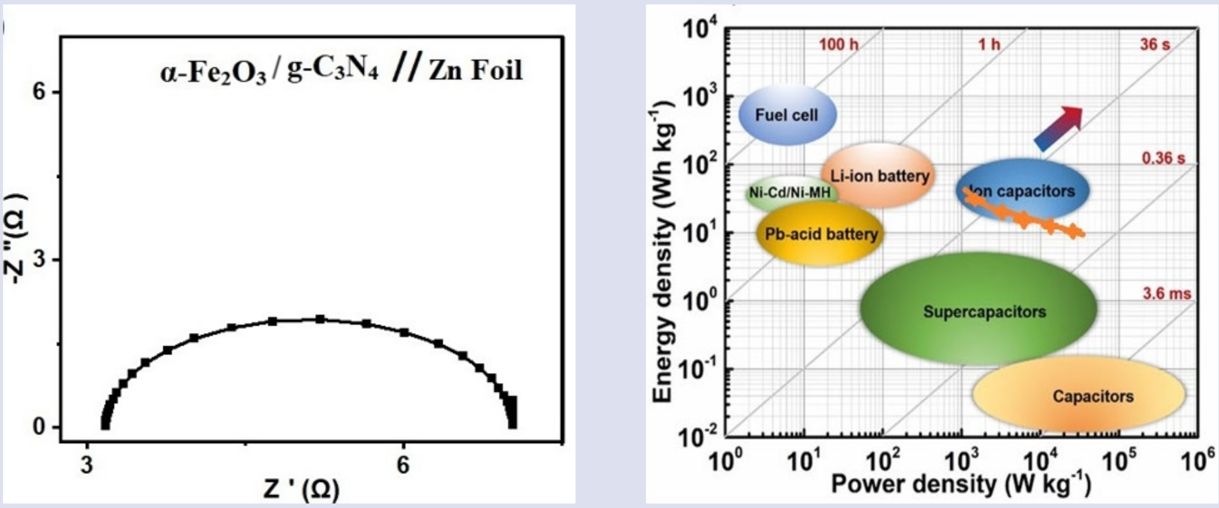

(a) (b)

Figure 8. (a) Nyquist plots at low frequency, (b) Ragone plot of the ZHSC

Table 1. Energy and power densities of the zinc ion hybrid supercapacitor at different current densities

Energy density/Power density (ED/PD) (Wh kg^{-1}/ W kg^{-1})					
Current density	2.5 Ag^{-1}	5 Ag^{-1}	10 Ag^{-1}	20 Ag^{-1}	40 Ag^{-1}
Energy density	38.8	27.7	19.4	16.6	11.1
Power density	1250	2500	5000	10.000	20.000

Table 2. Comparative Device Performance of Previously Reported α-Fe_2O_3 Energy Storage Devices

#	Device configuration	SC (Device)	Electrolyte	Potential range (V)	ED (Wh kg^{-1})	PD (W kg^{-1})	Stabilty (%) /cycles	Ref.
1	α-Fe_2O_3@CDs // 2 M KOH // BiOCl (ASC)	251 F g^{-1} at 1 Ag^{-1}	2M KOH	0-1.8 V	28	383	83/ 10.000	[15]
2	MoO_3-Fe_2O_3//AC [2]	216.7 F g^{-1} at 1 A g^{-1}	3M KOH	0-1.2	43.3	600	81.17/ 2.000	[34]
3	RGO // α-Fe_2O_3@CeO_2 (ASC)	50 F g^{-1} at 0.5Ag^{-1}	2M Na_2SO_4	0-1.5	15.62	781	87.5/ 2.000	[35]
4	α-Fe_2O_3/MnO_2/rGO//rGO (ASC)	97 F g^{-1} at 1 A g^{-1}	PVA/KOH gel-electrolyte	0-1.4	26.4	2099	91/ 5.000	[36]
6	Fe_2O_3@Ni1Co1-S//AC (ASC)	123.1 F g^{-1} at 1 Ag^{-1}	3 M KOH	0-1.6	43.8	810	92.4/ 10.000	[37]
7	α-Fe_2O_3/NiO/rGO // AC [2]	130 F g^{-1} at 1 A g^{-1}	6 M KOH	0-1.4	35.38	558	94.52/ 5.000	[38]
8	α-Fe_2O_3// NiO (ASC)	228.8 mF cm^{-2} at mA cm^{-2}	PVA/KOH gel-electrolyte	0-1.25	12.4	312	85 / 10.000	[39]
9	Fe_2O_3-P//MnO_2 (ASC)	-----	1M Na_2SO_4	0-1.6	57.3	1404	88/ 9.000	[40]
10	α-Fe_2O_3/g-C_3N_4 // Zn Foil	280 F g^{-1} at 2.5 A g^{-1}	2M KOH + 0.05 M $ZnSO_4$	1.0-2.0	38.8	1250	74/ 10.000	This work

Conclusions

To summarize, the purpose of this research was to investigate the electrochemical characteristics of g-C_3N_4 doped α-Fe_2O_3 for ZHSC applications. In the first step the composite material analyzed was done in three-electrode set up after the maximum conditions were optimized. Thereafter, the best yielded α-Fe_2O_3/g-C_3N_4 material was formed as cathode for ZHSC device when zinc foil was the both anode, and current collector. The performed ZHSC device ably reached the potential window of 2.0 volts with a high Sc of 280 F g^{-1} at a current density of 2.5 A g^{-1}. Additionally, the obtained maximum Ed and Pd were 38.8 Wh kg^{-1} and 20 kW kg^{-1}, respectively. This enhanced cell shows promise when compared to previous studies in the literature, as it exhibits a better power density with a wider working potential than asymmetric supercapacitors. Moreover, owing to these remarkable results, α-Fe_2O_3/g-C_3N_4 might be considered an appealing option for the cathode material in ZHSC.

Acknowledgements

This work was supported by the Research Fund of the Erciyes University (Project Number: 11978).

Conflicts of interest

There are no conflicts of interest in this work.

References

[1] Sharifi S., Rahimi K., Yazdani A., Highly Improved Supercapacitance Properties Of Mnfe$_2$o$_4$ Nanoparticles By Mos$_2$ Nanosheets, *Sci. Rep.,* 11 (1) (2020) 8378.

[2] Lazarte J.P.L., Dipasupil R.C., Pasco G.Y.S., Eusebio R.C.P., Orbecido A.H., Doong R.-A., Bautista-Patacsil L., Synthesis Of Reduced Graphene Oxide/Titanium Dioxide Nanotubes (Rgo/Tnt) Composites As An Electrical Double Layer Capacitor, *Nanomater,* 8(11) (2018) 934.

[3] Yetiman S., Pecenek H., Dokan F.K., Onses M.S., Yılmaz E., Sahmetlioglu E., Microwave-Assisted Fabrication Of High-Performance Supercapacitors Based On Electrodes Composed Of Cobalt Oxide Decorated With Reduced Graphene Oxide And Carbon Dot, *J. Energy Storage* , 49 (2022) 104103.

[4] El Ghazaly A., Zheng W., Halim J., Tseng E.N., Persson P.O., Ahmed B., Rosen J., Enhanced Supercapacitive Performance Of Mo1. 33c Mxene Based Asymmetric Supercapacitors In Lithium Chloride Electrolyte, *J. Energy Storage,* 41 (2021) 203-208.

[5] Yetiman S., Karagoz S., Kilic Dokan F., Onses M.S., Yilmaz E., Sahmetlioglu E., Rational Integration Of Zif-8 And Bipo(4) For Energy Storage And Environmental Applications, *Acs. Omega*, 7(49) (2022) 44878-44891.

[6] Şahan H., Ateş M.N., Dokan F.K., Ülgen A., Patat Ş., Synergetic Action Of Doping And Coating On Electrochemical Performance Of Lithium Manganese Spinel As An Electrode Material For Lithium-Ion Batteries, *B. Mater Sci.* , 38 (2015) 141-149.

[7] Mateen, A., Ansari, M.Z., Abbas, Q., Muneeb, A., Hussain, A., Eldin E.T., Alzahrani F.M., Alsaiari N.S., Ali S., Javed M.S., In Situ Nitrogen Functionalization Of 2d-Ti$_3$c$_2$t X-Mxenes For High-Performance Zn-Ion Supercapacitor, *Molecules*, 27 (21) (2022) 7446.

[8] Mateen A., Javed M.S., Khan S., Saleem A., Majeed M.K., Khan A.J., Tahir M.F., Ahmad M.A., Assiri M.A., Peng K.-Q., Metal-Organic Framework-Derived Walnut-Like Hierarchical Co-O-Nanosheets As An Advanced Binder-Free Electrode Material For Flexible Supercapacitor, *J. Energy Storage* , 49 (2022) 104150.

[9] Mateen A., Zubair M., Saleem M., Golubenkova A., Voskressensky L., Alothman A.A., Ouladsmane M., Ahmad A., Javed M.S., A Novel High-Performance Anode Material With An Enlarged Potential Window For A Hybrid Energy Storage System, *Energies*, 15 (24) (2022) 9577.

[10] Hussain S.K., Dudem B., Yu J.S., Enhanced Electrochemical Performance Via Ppy Encapsulated 3d Flower-Like Bismuth Molybdate Nanoplates For High-Performance Supercapacitors , *Appl. Surf. Sci.* , 478 (2019) 846-856.

[11] Yetiman S., Dokan F.K., Onses M.S., Yılmaz E., Sahmetlioglu E., Hybrid Electrodes Composed Of Graphitic Carbon Nitride And Zeolitic Imidazolate Framework-67 For Supercapacitor Applications, *Int. J. Energy Res.,* 46 (15) (2022) 22730-22743.

[12] Kiliç Dokan F., Şahan H., Özdemır B. Özdemır, N. Patat, Ş. Synthesis And Characterization Of Spinel Li$_4$ti$_5$o$_{12}$ Anode Material By Ctab Assisted Sol-Gel Method, *Acta Phys. Pol. A*, 125 (2) (2014) 648-649.

[13] Şahan H., Dokan F.K., Ülgen A., Patat Ş., Improvement Of Cycling Stability Of Limn$_2$o$_4$ Cathode By Fe$_2$o$_3$ Surface Modification For Li-Ion Battery ,*Ionics,* 20 (2014) 323-333.

[14] Patat S., Rahman S., Dokan F.K., The Effect Of Sodium And Niobium Co-Doping On Electrochemical Performance Of Li$_4$ti$_5$o$_{12}$ As Anode Material For Lithium-Ion Batteries, *Ionics,* 28 (7) (2022) 3177-3185.

[15] Yetiman S., Dokan F.K., Onses M.S., Huang, X., Yılmaz, E., Sahmetlioglu, E., Asymmetric And Zinc-Ion Hybrid Supercapacitors Based On Iron Oxide And Carbon Dots, *J. Energy Storage,* 68 (2023) 107608.

[16] Abbas Q., Mateen A., Khan A.J., Eldesoky G.E., Idrees A., Ahmad A., Eldin E.T., Das H.T., Sajjad M., Javed M.S., Binder-Free Zinc–Iron Oxide As A High-Performance Negative Electrode Material For Pseudocapacitors, *Nanomaterials*, 12 (18) (2022) 3154.

[17] Liu P., Fan X., Ouyang B., Huang Y., Hao R., Gao S., Liu W., Liu K., A Zn Ion Hybrid Capacitor With Enhanced Energy Density For Anode-Free, *J. Power Sources,* 518 (2022) 230740.

[18] Ji H., Jing X., Xu Y., Yan J., Li H., Li Y., Huang L., Zhang Q., Xu, H., Li, H., Magnetic Gc$_3$n$_4$/Nife$_2$o$_4$ Hybrids With Enhanced Photocatalytic Activity, *Rsc Advances,* 5 (71) (2015) 57960-57967.

[19] Xu M., Han L., Dong S., Facile Fabrication Of Highly Efficient G-C$_3$n$_4$/Ag$_2$o Heterostructured Photocatalysts With Enhanced Visible-Light Photocatalytic Activity, *Acs Appl. Mater. Interfaces,* 5 (23) (2013) 12533-12540.

[20] Zhou S.-X., Tao X.-Y., Ma J., Guo L.-T., Zhu Y.-B., Fan H.-L., Liu, Z.-S., Wei, X.-Y., Synthesis Of Flower-Like Pani/G-C$_3$n$_4$ Nanocomposite As Supercapacitor Electrode, *Vacuum*, 149 (2018) 175-179.

[21] Ragupathi, V., Panigrahi P., Subramaniam N.G., G-C$_3$n$_4$ Doped Mns As High Performance Electrode Material For Supercapacitor Application ,*Mater. Lett,* 246 (2019) 88-91.

[22] Li J., Chen D., Wu Q., A-Fe2o3 Based Carbon Composite As Pure Negative Electrode For Application As Supercapacitor, *Eur. J. Inorg. Chem.,* 2019 (10) (2019) 1301-1312.

[23] Song G., Chu Z., Jin W., Sun H., Enhanced Performance Of G-C_3n_4/Tio_2 Photocatalysts For Degradation Of Organic Pollutants Under Visible Light*, Chin. J. Chem. Eng,* 23(8) (2015) 1326-1334.

[24] Jiang H., Ma H., Jin Y., Wang L., Gao F., Lu Q., Hybrid A-Fe_2o_3@ Ni (Oh) $_2$ Nanosheet Composite For High-Rate-Performance Supercapacitor Electrode*, Sci. Rep ,* 6 (1) (2016) 31751.

[25] Zheng Y., Zhang X., Zhao J., Yang P., Assembled Fabrication Of A-Fe_2o_3/Biocl Heterojunctions With Enhanced Photocatalytic Performance*, Appl. Surf. Sci,* 430 (2018) 585-594.

[26] Nabi G., Riaz K.N., Nazir M., Raza W., Tahir M.B., Rafique M., Malik N., Siddiqa A., Gillani S.S.A., Rizwan M., Cogent Synergic Effect Of Tis_2/G-C_3n_4 Composite With Enhanced Electrochemical Performance For Supercapacitor*, Ceram. Int. Ceramics* , 46 (17) (2020) 27601-27607.

[27] Palanivel B., Hossain M.S., Macadangdang Jr, R.R., Ayappan C., Krishnan V., Marnadu R., Kalaivani T., Alharthi, F.A., Sreedevi G., Activation Of Persulfate For Improved Naproxen Degradation Using $Feco_2o_4$@ G-C_3n_4 Heterojunction Photocatalysts*, Acs Omega,* 6(50) (2021) 34563-34571.

[28] Chen X., Kuo D.-H., Lu D., Nanonization Of Gc_3n_4 With The Assistance Of Activated Carbon For Improved Visible Light Photocatalysis, *Rsc Adv.,* 6 (71) (2016) 66814-66821.

[29] Kumbul A., Gokturk E., Sahmetlioglu E.,Synthesis, Characterization, Thermal Stability And Electrochemical Properties Of Ortho-Imine-Functionalized Oligophenol Via Enzymatic Oxidative Polycondensation*, J. Polym. Res*., 23 (2016) 1-11.

[30] Turac E., Sahmetlioglu E., Toppare L., Yuruk H., Synthesis, Characterization And Optoelectrochemical Properties Of Poly (2, 5-Di (Thiophen-2-Yl-) 1-(4-(Thiophen-3-Yl) Phenyl)-1h-Pyrrole-Co-Edot)*, Des. Monomers Polym. ,* 13(3) (2010) 261-275.

[31] Turac E., Sahmetlioglu E., Demircan A., Toppare L., Synthesis And Characterization Of Conducting Copolymer Of Trans-1-(4-Methyl-3′-Thienyl)-2-(Ferrocenyl) Ethene With Edot*, J. Appl. Polym. Sci.,* 126 (3) (2012) 808-814.

[32] Zhu Q., Zhao D., Cheng M., Zhou J., Owusu K.A., Mai L., Yu Y., A New View Of Supercapacitors: Integrated Supercapacitors, *Adv. Energy Mater.,* 9(36) (2019) 1901081.

[33] Zhang L., Wu D., Wang G., Xu Y., Li H., Yan X., An Aqueous Zinc-Ion Hybrid Super-Capacitor For Achieving Ultrahigh-Volumetric Energy Density*, Chin. J. Chem.,* 32(2) (2021) 926-931.

[34] Sundaresan S., Subramanian D., Raju G., Exploration Of Two Dimensional Moo_3-Fe_2o_3 Nanocomposite For The Fabrication Of High Energy Density Supercapacitor Applications*, Inorg. Chem. Commun.,*148 (2023) 110360.

[35] Mazloum-Ardakani M., Sabaghian F., Yavari M., Ebady A., Sahraie N., Enhance The Performance Of Iron Oxide Nanoparticles In Supercapacitor Applications Through Internal Contact Of A-Fe_2o_3@Ceo_2 Core-Shell*, J. Alloys Compd.*, 819 (2020) 152949.

[36] Geerthana M., Prabhu S., Ramesh R., Hierarchical A-Fe_2o_3/Mno_2/Rgo Ternary Composites As An Electrode Material For High Performance Supercapacitors Application*, J. Energy Storage*, 47 (2022) 103529.

[37] Guo M., Sun J., Liu Y., Huangfu C., Wang R., Han C., Qu Z., Wang N., Zhao L., Zheng Q., Optimizing Fe_2o_3-Based Supercapacitor Cathode With Tunable Surface Pseudocapacitance Via Facile In Situ Vulcanization Process*, J. Electroanal. Chem.,* 901 (2021) 115785.

[38] Mummoorthi G., Shajahan S., Abu Haija M., Mahalingam U., Rajendran R., Synthesis And Characterization Of Ternary A-Fe_2o_3/Nio/Rgo Composite For High-Performance Supercapacitors*, Acs Omega*, 7(31) (2022) 27390-27399.

[39] Zhang S., Yin B., Wang Z., Peter F., Super Long-Life All Solid-State Asymmetric Supercapacitor Based On Nio Nanosheets And A-Fe_2o_3 Nanorods*, J. Chem. Eng.*, 306 (2016) 193-203.

[40] Liang H., Xia C., Emwas A.-H., Anjum D.H., Miao X., Alshareef H.N., Phosphine Plasma Activation Of A-Fe_2o_3 For High Energy Asymmetric Supercapacitors*, Nano Energy,* 49 (2018) 155-162.